

## Article

# Effect of NO<sub>x</sub> and SO<sub>x</sub> Contaminants on Corrosion Behaviors of 304L and 316L Stainless Steels in Monoethanolamine Aqueous Amine Solutions

Eleni Lamprou <sup>1</sup>, Fani Stergioudi <sup>1,\*</sup>, Georgios Skordaris <sup>2</sup>, Nikolaos Michailidis <sup>1</sup>, Evie Nessi <sup>3</sup>, Athanasios I. Papadopoulos <sup>3</sup> and Panagiotis Seferlis <sup>3,4</sup>

<sup>1</sup> Physical Metallurgy Laboratory, Mechanical Engineering Department, Aristotle University of Thessaloniki, 54124 Thessaloniki, Greece

<sup>2</sup> Laboratory for Machine Tools and Manufacturing Engineering, Mechanical Engineering Department, Aristotle University of Thessaloniki, 54124 Thessaloniki, Greece

<sup>3</sup> Chemical Process and Energy Resources Institute, Centre for Research and Technology Hellas, 57001 Thermi, Greece

<sup>4</sup> Laboratory of Machine Dynamics, Mechanical Engineering Department, Aristotle University of Thessaloniki, 54124 Thessaloniki, Greece

\* Correspondence: fstergio@auth.gr

**Abstract:** This work is devoted to evaluating the corrosion behaviors of SS 304L and SS 316L in monoethanolamine solutions (MEA) containing SO<sub>x</sub> and NO<sub>x</sub> pollutants, examining both lean and CO<sub>2</sub>-loaded conditions at 25 °C and 40 °C. Electrochemical techniques (potentiodynamic and cyclic polarization) were used along with Scanning Electron Microscopy, Confocal Microscopy and weight loss measurements. The results reveal that the introduction of SO<sub>x</sub> and NO<sub>x</sub> pollutants increased the corrosion rate, whereas CO<sub>2</sub> loading primarily reduced the corrosion resistance in the lean MEA solution, while its impact on solutions with SO<sub>x</sub> and NO<sub>x</sub> was less pronounced. This suggests that SO<sub>x</sub> and NO<sub>x</sub> play primary roles in the metal's dissolution. Also, SS 316L demonstrated superior corrosion resistance compared to 304L in nearly all of the cases examined. Elevated temperatures were also found to intensify the corrosion rate, indicating a correlation between the corrosion rate and temperature. A microscopic observation and EDX analysis revealed that corrosion products are characterized by high concentrations of iron (Fe) and oxygen (O) as well as carbon (C). There is also an indication of the possible formation of amine complexes, suggesting a potential for amine degradation. No pitting corrosion was observed in SS 304L and SS 316L across any tested solution. Finally, the immersion results expose a tendency for passivity in all amine solutions and at both temperatures after several days of exposure. Moreover, they confirm the very low corrosion rate calculated from potentiodynamic curves due to minimal weight loss after 24 days of immersion.



**Citation:** Lamprou, E.; Stergioudi, F.; Skordaris, G.; Michailidis, N.; Nessi, E.; Papadopoulos, A.I.; Seferlis, P. Effect of NO<sub>x</sub> and SO<sub>x</sub> Contaminants on Corrosion Behaviors of 304L and 316L Stainless Steels in Monoethanolamine Aqueous Amine Solutions. *Coatings* **2024**, *14*, 842. <https://doi.org/10.3390/coatings14070842>

Academic Editor: Paolo Castaldo

Received: 4 June 2024

Revised: 30 June 2024

Accepted: 2 July 2024

Published: 5 July 2024



**Copyright:** © 2024 by the authors. Licensee MDPI, Basel, Switzerland. This article is an open access article distributed under the terms and conditions of the Creative Commons Attribution (CC BY) license (<https://creativecommons.org/licenses/by/4.0/>).

**Keywords:** MEA; corrosion; CO<sub>2</sub> caption; microstructure

## 1. Introduction

Currently, carbon dioxide emissions stand as one of the most significant challenges that our society is called upon to confront. These emissions are primarily generated from human activities, with the foremost example being the combustion of solid, liquid and gaseous fossil fuels. In addition to CO<sub>2</sub> emissions, by-products of combustion processes such as SO<sub>x</sub> and NO<sub>x</sub> are also discharged into the atmosphere [1,2]. All of these emissions contribute to the worsening of climate change and to global warming, especially in an era where human energy demands are constantly on the rise [3]. One promising approach to mitigate the adverse consequences of these emissions involves the post-combustion capture of acid gasses using alkanolamine-based chemical solvents [4] owing to their high absorption rate, substantial absorption capacity and the capability for regeneration [5].

Monoethanolamine is the most prevalent amine solvent employed in such capture processes due to its numerous advantages over other types of amines [6–9].

Despite the fact that amines are not intrinsically corrosive, since they have both high alkalinity and low conductivity, corrosion issues have been extensively documented in power plants. Corrosion of the process components is one of the most serious operational concerns because it not only reduces the lifespan of critical infrastructure but also poses significant safety risks due to potential equipment failure [10–13]. The presence of CO<sub>2</sub> and H<sub>2</sub>O has been found to be the main contributor to the high corrosiveness of amine solutions due to the reactions they promote, causing the formation of oxidizing agents, with the most prominent being HCO<sub>3</sub><sup>−</sup>, H<sub>3</sub>O<sup>+</sup> and H<sub>2</sub>O [6,14,15]. When these agents interact with a metal substrate, a potential difference arises between them, initiating a charge transfer mechanism that leads to metal dissolution. Besides CO<sub>2</sub> loading, MEA is considered highly corrosive when impurities such as SO<sub>x</sub>, NO<sub>x</sub>, fly ash and hydrogen sulfide (H<sub>2</sub>S) are present in the solution. In particular, recent studies have shown that the presence of SO<sub>x</sub> contaminants can deteriorate the corrosion resistance of steels by promoting both anodic and cathodic reactions [16].

The corrosion rate of amine solvents is influenced by various factors, including the amine's structure, solution temperature, amine concentration, acidity and pH levels, along with the formation of a passive layer [11,14,17,18]. Different combinations of these parameters can lead to dissimilar corrosion mechanisms. This complexity within the system makes it challenging to converge on a single, unified corrosion model [11].

To date, the most common construction material used in power plants for post-combustion CO<sub>2</sub> capture is carbon steel, primarily due to its low cost. However, significant corrosion problems have led to a recent focus on using alternative materials like stainless steels in certain parts of the capture unit to control corrosion. Despite the limited literature on the corrosion behavior of stainless steels in amine systems [19], some studies have confirmed that stainless steels perform well in MEA amine solutions [20], often outperforming carbon steel [19,21].

Although several studies have been published examining the MEA-H<sub>2</sub>O-CO<sub>2</sub> system and the corrosion mechanism underlying it, there is a significant research gap concerning the MEA-H<sub>2</sub>O-CO<sub>2</sub>-SO<sub>x</sub>-NO<sub>x</sub> mixture. Understanding the effects of these compounds on corrosion performance is pivotal for maintaining the integrity and longevity of crucial industrial infrastructure by developing effective strategies to mitigate corrosion issues, thereby ensuring the reliability and safety of power plants.

The objective of the present study is to evaluate the corrosion behaviors of 304L and 316L stainless steels under various environmental conditions using amine solutions as the corrosive medium. These stainless steels were selected for their potential suitability as alternatives to carbon steel in power plants. The tested solutions were composed of MEA-based solvents containing sulfuric acid (H<sub>2</sub>SO<sub>4</sub>) and nitric acid (HNO<sub>3</sub>) in lean conditions or loaded with CO<sub>2</sub> and were investigated at temperatures of 25 °C and 40 °C. This addition to the literature aims to simulate the presence of pollutants like SO<sub>x</sub> and NO<sub>x</sub>, which are typically found in flue gas emissions. This study employed a range of electrochemical techniques, including open circuit potential measurements (OCP), potentiodynamic curves, and cyclic polarization curves, in order to elucidate the effects of SO<sub>x</sub> and NO<sub>x</sub> pollutants in corrosion behavior. These techniques provide crucial data on corrosion parameters, including the corrosion current, potential and rate, allowing for a better understanding of the underlying corrosion mechanisms. Scanning Electron Microscopy (SEM) in combination with an Energy-Dispersive X-ray Spectroscopy (EDX) analysis was utilized to examine the microstructural characteristics of the corroded specimens. This analysis enables a thorough assessment of the extent of material degradation and provides insights into how the microstructure of the material has been affected by the corrosion process. Also, weight loss measurements were carried out to investigate the impact of prolonged exposure to corrosive solutions on the specimens. Finally, three-dimensional measurement facilities

of the confocal microscope SURF of NANOFOCUS AG (Oberhausen, Germany) were employed to evaluate the surfaces of the corroded samples.

## 2. Materials and Methods

To carry out the electrochemical experiments and the weight loss measurements, stainless steels 304L and 316L were used. Materials' chemical compositions are reported in Table 1.

**Table 1.** Chemical compositions (wt%) of SS 304L and 316L used in experiments.

%	C	Cr	Mn	Si	P	Ni	S	Mo	Fe
SS 304L	0.03	18	2	1	0.0045	8	0.03	-	Bal.
SS 316L	0.022	17.5	1.8	-	0.003	10	0.54	2	Bal.

Small coupons of stainless steel alloys were cut from a rod with a diameter and a height of 6 mm and 10 mm, respectively. Before undergoing testing, all samples were subjected to a pretreatment process, which included mechanical polishing using silicon carbide (SiC) papers ranging from 800 to 1200 grit, both on the flat surface of the sample and around its perimeter, rinsing with distilled water and ethanol and finally drying, according to ASTM Standard G1-03 [22]. This procedure is employed to ensure that the specimen's surface does not influence the corrosion properties being measured.

All of the electrochemical tests were performed using a three-electrode setup with a saturated calomel electrode (SCE) serving as the reference electrode and a platinum rod as the counter one. The experiments were controlled with a VoltaLab PGZ 402 Potentiometer from the Radiometer Analytical company (Villeurbanne Cedex, France). Experiments were carried out at two different temperatures, 25 °C and 40 °C, under atmospheric pressure. These conditions were selected in order to simulate the real operating conditions encountered in the capture units.

Prior to each electrochemical experiment, the open circuit potential (OCP) of the specimens was recorded until a steady-state value was achieved. A scanning rate of 2 mV/s was applied to all of the polarization measurements, with the cathode-to-anode scanning range being set from –800 mV to +900 mV (versus SCE) relative to the OCP value. Following the experiments, the Tafel extrapolation method was applied to determine key corrosion parameters such as corrosion current, potential, and the slopes of cathodic and anodic curves. These parameters were derived from measurements taken at potentials deviating more than 50 mV from the rest of the potentials and extending up to 350 mV. Multiple calculations of each parameter were performed to maintain a satisfactory level of accuracy. In the cyclic polarization tests, the potential was reversed when a value of 900 mV (versus SCE) was reached and/or the hysteresis loop was completed. Each electrochemical experiment was carried out at least three times to assess the results' consistency.

To conduct the weight loss measurements at 25 °C and 40 °C, stainless steel coupons similar to those used in the electrochemical experiments were employed. Before each experiment, a predefined volume of solution consisting of 100 mL was measured and placed in an isolated container. After 3, 7, 12 and 24 days of exposure, the specimens were removed, cleaned in a water bath and dried. The final mass was measured.

Analysis of the samples was conducted using Scanning Electron Microscopy (SEM), (Phenom ProX desktop SEM, Thermo Fisher Scientific, Eindhoven, The Netherlands) equipped with Energy-Dispersive X-ray Spectroscopy (EDX) analyzer, used to determine the elemental compositions of the observed regions and morphologies. In this way, a clearer picture of the corrosion mechanism could be achieved.

### Amine Solvent Preparation

The amine solvents used were prepared by diluting 99 wt.% MEA amine with deionized water to achieve a final amine content of 30 wt.%. The CO<sub>2</sub> loading was 0.5 mol

$\text{CO}_2/\text{mol MEA}$ . To simulate solvent contamination by  $\text{SO}_X$  and  $\text{NO}_X$  pollutants, which are commonly found in flue gas, relevant amounts of sulfuric ( $\text{H}_2\text{SO}_{4(\text{aq})}$ ) and nitric acid ( $\text{HNO}_{3(\text{aq})}$ ) were added at a concentration of 0.06 mol pollutants/mol MEA. Specifically, the mole ratio between sulfuric and nitric acid is  $[\text{mol H}_2\text{SO}_4]/[\text{mol HNO}_3] = 4$ .

Solutions of 30 wt.%  $\text{MEA}_{(\text{aq})}$  with  $\text{SO}_3^-$  and  $\text{NO}_3^-$  contaminants were prepared in the lab by weighing the respective amounts of MEA, water,  $\text{H}_2\text{SO}_4$  and  $\text{HNO}_3$  with the aid of a precision scale. The solutions were subsequently transferred to a dedicated setup via a pump to react with  $\text{CO}_2$  (Figure 1). More specifically, a batch of contaminated  $\text{MEA}_{(\text{aq})}$  (2 L) was bubbled with pure  $\text{CO}_2$  at 40 °C until the targeted loading was achieved. According to the experimental procedure, the solution was stirred and heated up to the targeted temperature while being degassed with  $\text{N}_2$  to expel diluted oxygen. Then, a pure  $\text{CO}_2$  stream of controlled flow (1 L/min total) was supplied until equilibrium solubility was achieved. Equilibrium was considered when the exiting gas flow rate was equal to the entering rate, as monitored by a gas flow meter. Samples of the liquid were collected for analysis. The  $\text{CO}_2$  loading was quantified by  $\text{BaCO}_3$  precipitation, and the amine content was measured by  $\text{NaOH}-\text{HCl}$  titrations [23]. The solution was then subjected to a corrosion study.

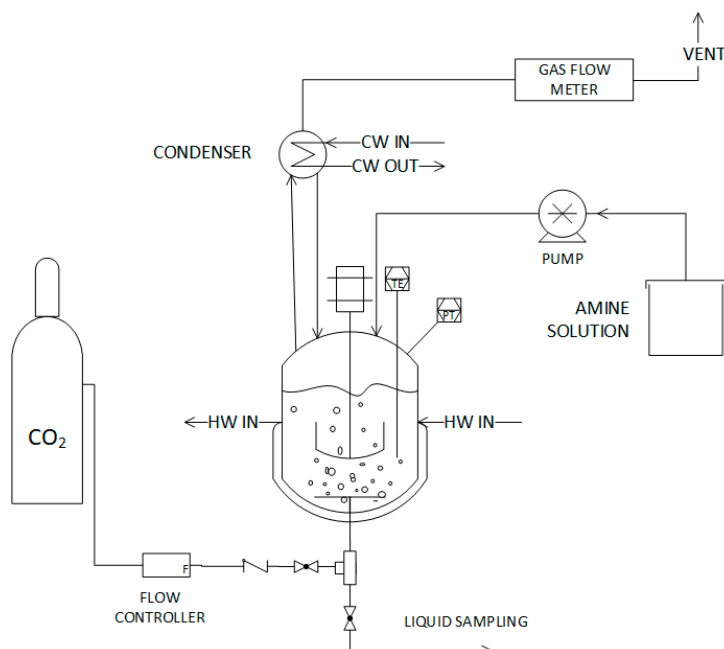


**Figure 1.** Simplified diagram of amine loading setup.

### 3. Results and Discussion

#### 3.1. Potentiodynamic Polarization Measurements

Figure 2 illustrates typical potentiodynamic polarization curves obtained from SSs 304L and 316L samples immersed in various MEA solutions, either lean or loaded with  $\text{CO}_2$ , at the temperatures of 25 °C and 40 °C. Table 2 presents the electrochemical values determined by the Tafel extrapolation method.

As shown in Figure 2, all of the anodic polarization curves exhibit the same behavior, characterized by the presence of three distinct regions. At the initial stage, an active corrosion behavior is observed (area I), indicative of metal dissolution, which ends with an abrupt decrease in the corrosion current density. The active area of each curve extends from the corresponding value of  $E_{\text{corr}}$  to approximately 500 mV. The reduction in current density is followed by a passivation stage where the current stabilizes and becomes voltage independent (area II) owing to the deposition or absorption of corrosion products on the metal surface. Generally, in all cases, the limited potential range of the passivation area implies that there is a corrosion layer that might be too thin, discontinuous or un-

stable so it may fail to provide efficient protection to the substrate. The passive region in amine solutions containing  $\text{SO}_X$  or  $\text{SO}_X$  and  $\text{NO}_X$  lies in the same potential amplitude of 500–700 mV compared to MEA with no pollutants, which has a passive region that extends from approximately 500 to 900 mV, indicating that the passive film is of the same nature. Also, the addition of  $\text{SO}_X$  and  $\text{NO}_X$  increased the passive current density, signifying that the presence of these impurities reduced the protectiveness ability of the corrosion product layer covering the metal surface, mainly at 40 °C [17]. Finally, the passive region is succeeded by a steep increase in the current density, attributed either to the dissolution of a barrier film permeable to ions or to the corrosion of areas on the metal that have not been covered by corrosion products.

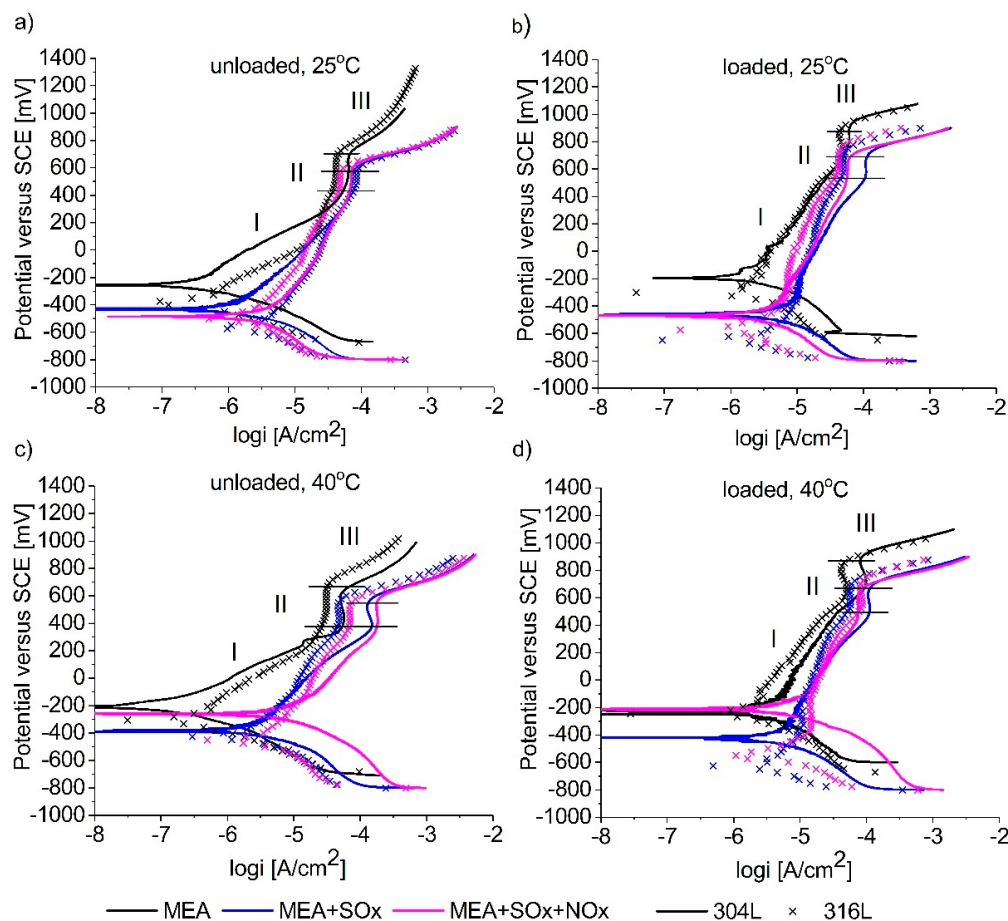


**Figure 2.** Potentiodynamic polarization plots of SSs 304L and 316L immersed in (a,b) unloaded and loaded MEA solutions at 25 °C and (c,d) unloaded and loaded MEA solutions at 40 °C.

It can be noticed that the introduction of  $\text{SO}_X$  and  $\text{NO}_X$  pollutants shifts the polarization curves towards higher anodic currents, whether the solution is lean or loaded and regardless of temperature, in both SS 304L and SS 316L. This shift signifies that stainless steels have reduced corrosion resistance when immersed in these solutions. Indeed, as derived from the corrosion rate calculation in Table 2, when  $\text{SO}_X$  and  $\text{NO}_X$  pollutants are added in a MEA solvent, the corrosion rate increases, indicating that the amine becomes more aggressive with the presence of pollutants. It has also been confirmed from other studies that the addition of  $\text{SO}_X$  and  $\text{NO}_X$  has a profound impact on the corrosion rate within aqueous solutions [24]. When  $\text{CO}_2$  is added to the pure MEA solution, the corrosion rate increases significantly. Conversely, the addition of  $\text{CO}_2$  in amine solutions containing pollutants does not notably increase the corrosion rate, implying that carbon dioxide has a minimal impact on the solution's corrosive nature. On the contrary, it seems that  $\text{SO}_X$

and NO<sub>x</sub> impurities are the primary contributors to increased metal dissolution. A more detailed explanation about this will be discussed in a paragraph below.

**Table 2.** Calculation data extracted from Tafel extrapolation for SSs 304L and 316L: corrosion potential ( $E_{corr}$ ), corrosion current density ( $I_{corr}$ ), anodic and cathodic slopes ( $\beta_a$  and  $\beta_c$ ) and corrosion rates and passive current density ( $I_{passive}$ ) in all amine solutions tested at 25 °C and 40 °C.

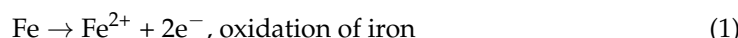
Amine Type	$E_{corr}$ [mV vs. SCE] 25 °C/40 °C	$I_{corr}$ [ $\mu\text{A}/\text{cm}^2$ ] 25 °C/40 °C	$\beta_c$ [mV] 25 °C/40 °C	$\beta_a$ [mV] 25 °C/40 °C	Cor. r. [ $\mu\text{m}/\text{Y}$ ] 25 °C/40 °C	$I_{passive}$ [ $\mu\text{A}/\text{cm}^2$ ] 25 °C/40 °C
SS 304L	Lean MEA	−374/−301	0.1/0.2	−205.7/−155.8	100/225	1.4/2.8
	Lean MEA with SO <sub>x</sub>	−431.4/−392.9	1.9/2.3	−234.6/−347.7	324.5/470.1	22.8/27.4
	Lean MEA with SO <sub>x</sub> /NO <sub>x</sub>	−570/−272.7	3.6/5.9	−233.9/−209.1	475.5/354.8	42.6/69.6
	Loaded MEA	−195.8/−229	1.45/4.5	−184.4/−278	444/960	28.1/47.6
	MEA loaded with SO <sub>x</sub>	−449.2/−475.7	2.8/3.9	−233.5/−312	277.6/787.8	32.8/45.4
	MEA loaded with SO <sub>x</sub> /NO <sub>x</sub>	−483.2/−218.7	3.9/4.4	−305.1/−168.5	529.7/225.6	45.3/51.9
SS 316L	Lean MEA	−393/−291	0.4/0.6	−155.7/−210.2	242/286.1	4.2/6.7
	Lean MEA with SO <sub>x</sub>	−570/−436	1.8/2.2	−171.5/−167	386.1/189.8	20.8/25
	Lean MEA with SO <sub>x</sub> /NO <sub>x</sub>	−505/−464	2.4/3.3	−319.3/−263.9	419.4/362.4	28.1/38.8
	Loaded MEA	−359/−256	0.9/2.5	−163.6/−267.5	309.4/425.1	10.9/29.5
	MEA loaded with SO <sub>x</sub>	−650/−626	2.1/2.7	−157.9/−236.7	109.9/189.8	24.5/31.8
	MEA loaded with SO <sub>x</sub> /NO <sub>x</sub>	−590/−568	2.5/3.5	−227.1/−148	358.4/220.5	29.7/40.7

Based on the analysis of corrosion rates, it is evident that SS 316L exhibits superior corrosion resistance compared to SS 304L across all examined cases. This fact is further confirmed by the observation that the anodic polarization curves of SS 304L are slightly shifted to higher current densities than SS 316L. The only exception arises in the case of the lean MEA solution at 25 °C and 40 °C, where SS 304L appears to have lower corrosion rates. Nonetheless, the differences in corrosion rates between SS 304L and SS 316L are relatively minor.

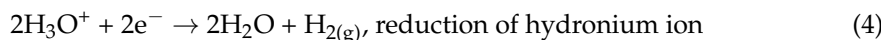
According to the experimental results for stainless steels 304L and 316L, changes in temperature notably affected the corrosion rates across all solutions examined. Increasing the solution temperature caused an acceleration in the corrosion rate. This could be attributed to the fact that at elevated temperatures, the reactions that lead to the formation of oxidizing agents occur with a faster rate, disturbing the equilibrium between metal dissolution and oxidizer reduction. To restore balance, more metal is dissolved, and thus, the corrosion rate is increased [9,25].

Generally, in MEA amine solutions, the primary anodic reaction is the dissolution of iron, while the main cathodic reactions contributing to metal dissolution are as follows [6,17]:

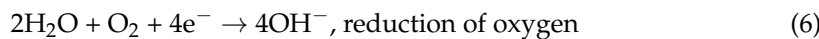
Anodic reaction:



Cathodic reactions:



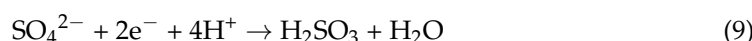
Under aerobic conditions, the reduction of oxygen is also possible, as shown in reaction (6):



The resulting precipitation products can be characterized as follows:



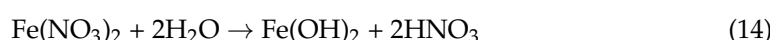
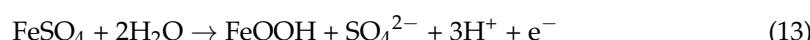
When sulfuric and nitric acids are introduced on the amine solvent, they undergo ionization due to the presence of water, resulting in the formation of sulfate ( $\text{SO}_4^{2-}$ ) and nitrate ( $\text{NO}_3^-$ ) anions.  $\text{SO}_4^{2-}$  and  $\text{NO}_3^-$  ions have greater standard electrode potentials than  $\text{Fe}^{2+}$  for the iron dissolution reaction and behave as oxidizing agents. By accepting electrons, they accelerate the dissolution of the metal substrate. Some indicative reactions are given in reactions 9 and 10 [26–29]. Information on further cathodic reactions can be found in reference [26].



Besides promoting cathodic reactions, sulfate and nitrate anionic species have a double contribution to corrosion. They react with iron cations ( $\text{Fe}^{2+}$ ) to produce ferrous sulfate ( $\text{FeSO}_4$ ) and ferrous (II) nitrate ( $\text{Fe}(\text{NO}_3)_2$ ), as shown in reactions (11) and (12).



The resulting compounds from reactions (11) and (12) can undergo further hydrolysis, regenerating  $\text{SO}_4^{2-}$  and  $\text{NO}_3^-$  anions, thus perpetuating the corrosion cycle. The hydrolysis reactions are presented in Equations (13) and (14).



In this manner, the formation and hydrolysis of ferrous compounds continuously generate new oxidizing agents, thereby sustaining and accelerating the corrosion of the metal substrate, leading to a faster corrosion rate [30].

In summary, it is evident that the presence of sulfuric and nitric acids plays a significant role in metal corrosion, creating a continuous loop where these acids keep producing oxidizing agents that maintain and accelerate the corrosion process. On the contrary,  $\text{CO}_2$  only contributes to corrosion by forming bicarbonate ions that cause metal oxidation. A schematic representation of the corrosion mechanism for SSs 304L and 316L is presented in Figure 3.

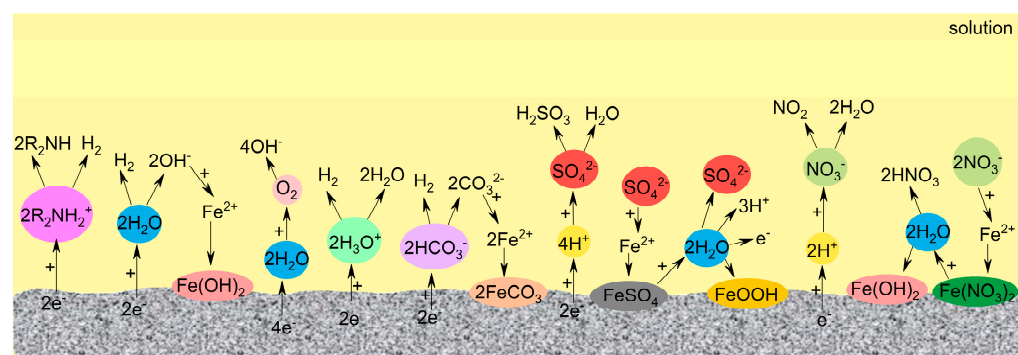


**Figure 3.** A schematic representation of the corrosion mechanism of SSs 304L and 316L when immersed in MEA-loaded solutions containing  $\text{SO}_x$  and  $\text{NO}_x$  pollutants.

### 3.2. Cyclic Polarization Measurements

Cyclic polarization is a valuable technique that is employed to assess the susceptibility of materials like stainless steel to localized corrosion in different aqueous amine solutions. Generally, this technique relies on several criteria to evaluate the material's resistance to localized corrosion. The first one is based on the presence of a hysteresis loop, which is formed by different current densities observed between reverse and forward scanning at the same potential. A negative hysteresis loop signifies a lower current density during the reverse scan than in the forward scan, indicating the material's reduced susceptibility to localized corrosion. The second criterion refers to the anodic to cathodic transition potential ( $E_{a/c\ tr}$ ), which is the potential of reverse scan at which the anodic current density shifts to the cathodic current density. When this potential is more noble than  $E_{corr}$ , it means that the material is not prone to localized corrosion or has the ability to easily restore its damaged oxide film. The third criterion is the difference in the current density between forward and reverse scanning. In the case of a negative loop, the greater the difference in current densities, the less vulnerable the material to pitting corrosion [31,32]. These standards provide valuable insights into the material's ability to resist localized corrosion based on the observed electrochemical behavior during cyclic polarization testing.

Figures 4 and 5 show the cyclic polarization curves for SSs 304L and 316L respectively, at 25 °C and 40 °C in various MEA solutions. All of the cyclic curves for both SS 304L and SS 316L exhibit a negative hysteresis loop along with an anodic to cathodic transition potential in the reverse scan which is more noble than the corresponding corrosion potential. Generally, these solvent types demonstrate similar resistance to localized corrosion (according to the criteria mentioned before), implying the robust resistance of 304L and 316L against pitting corrosion. However, an exception concerns SS 304L in the MEA solution containing SO<sub>x</sub> and NO<sub>x</sub> pollutants at 40 °C, both in lean and loaded conditions, where the hysteresis loop has a smaller area, probably signifying a reduced resistance in local corrosion (pitting) in this specific case. The sensitization to localized corrosion in SS 304L may be attributed to its microstructural difference since in SS 304L, a higher content of carbides precipitates is observed (Figure 4e). These can act as initiation sites for pitting.

### 3.3. Surface and Component Characterization of Corroded Specimens

After conducting potentiodynamic polarization tests, a thorough examination of the specimen surfaces was undertaken to elucidate the formation of corrosion products and to gain insights into the underlying corrosion mechanism.

Figure 6 illustrates an indicative microstructure of the SS 304L and SS 316L specimens tested in unloaded MEA-based solutions at 25 °C and 40 °C. In general, the microstructural characteristics of the corroded specimens for both stainless steels do not appear to show significant differences. In lean MEA solutions at both temperatures, the SEM images reveal the presence of few small, amorphous corrosion products dispersed across the corroded specimen's surface. The presence of these products was more pronounced in the case of amines containing SO<sub>x</sub> and NO<sub>x</sub> pollutants, clearly suggesting relatively higher corrosion rates. The EDX analysis confirmed a predominant composition of iron and oxygen, indicating the likely existence of oxide layers. Although an EDX analysis cannot precisely quantify the elemental percentages in each chemical compound, the high concentrations of certain elements strongly indicate their presence. However, further precise characterization using XRD or XPS is necessary to accurately identify the corrosion products. This investigation is planned as the next step in this research. These products are possibly formed due to the reaction of ferrous cations (Fe<sup>2+</sup>) with hydroxide (OH<sup>-</sup>) (reaction (7)) or from the dissolution of ferrous sulfate (FeSO<sub>4</sub>) and ferrous (II) nitrate (Fe(NO<sub>3</sub>)<sub>2</sub>), which gives FeOOH or Fe(OH)<sub>2</sub> (reactions (13) and (14)) [20].

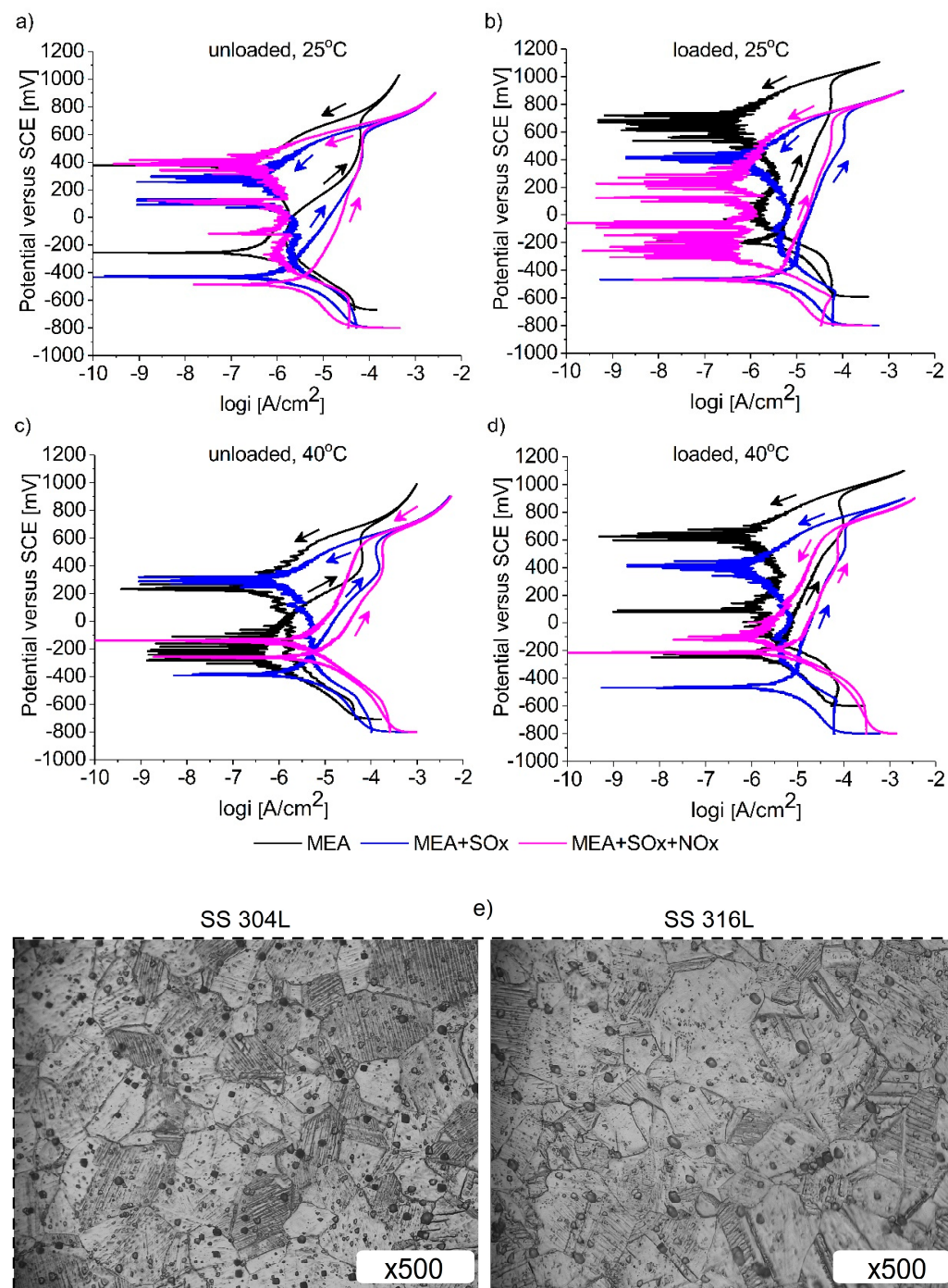


**Figure 4.** Cyclic polarization curves of SS 304L immersed in (a,b) unloaded and loaded MEA solutions at 25 °C, (c,d) unloaded and loaded MEA solutions at 40 °C and (e) microstructure of SS 304L and SS 316L in optical microscope.

Beyond the oxide layers, distinct black areas were also identified on the metal surface, primarily consisting of carbon, iron, oxygen and nitrogen. Given that nitrogen is an element contained in amine solvents, the presence of such compounds suggests the absorption of by-products in the metal substrate resulting from the decomposition of amine solution. It has been confirmed in other studies that MEA itself can react with iron to form the complex compound mentioned in references [33,34]. In particular, it is likely that the iron dissolves directly by replacing the hydrogen in the hydroxyl group of ethanolamine. Also, NO<sub>x</sub> species interact with amine to produce nitrosamines and nitramines [33,35],

which may further be combined with metal or metal ions to produce amine degradation products. Notably, these black layers exhibit a tendency to develop either above or below the iron precipitates.

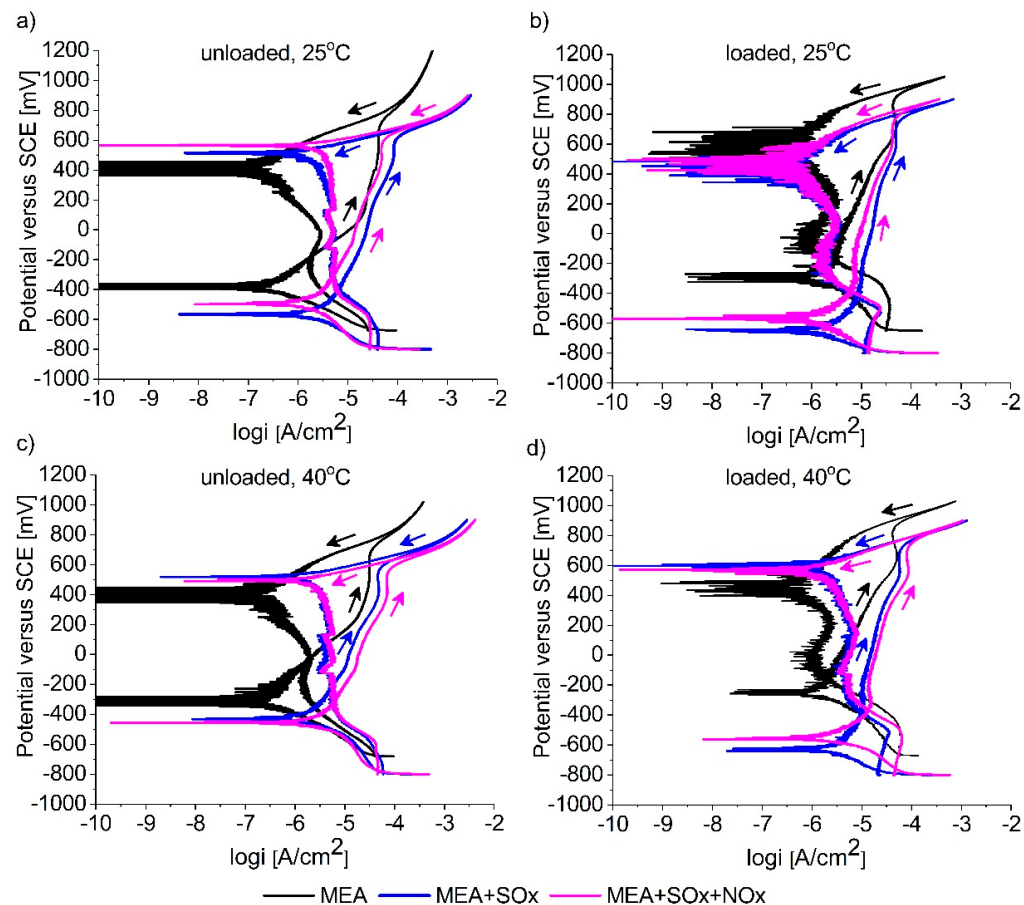


**Figure 5.** Cyclic polarization curves of SS 316L immersed in (a,b) unloaded and loaded MEA solutions at 25 °C and (c,d) unloaded and loaded MEA solutions at 40 °C.

Furthermore, a temperature-dependent trend emerged from the observations. At 40 °C, oxide and black layer formations intensified compared to the conditions at 25 °C, extending across an expanded region of the specimen's surface. This suggests a temperature-dependent effect on the corrosion process, which is consistent with the findings from the polarization curves.

Figure 7 depicts SEM images of specimens immersed in loaded MEA solutions. Polygonal white deposits rich in iron, oxygen and carbon were detected, attributed to the formation of siderite ( $\text{FeCO}_3$ ) (Figure 7a). The use of siderite film is considered an effective way to mitigate corrosion processes and protect the metal substrate [20,36]. Siderite is produced due to the reaction of ferrous anions ( $\text{Fe}^{2+}$ ) with carbonate ( $\text{CO}_3^{2-}$ ) (reaction 8).

Besides the presence of siderite, corrosion products and black layers were also observed in the corroded specimens (Figure 7b), similar to those found in the unloaded conditions. Additionally, the temperature increase resulted in a greater precipitation of corrosion products, covering a larger surface area. The fact that higher temperatures led to the increased formation of corrosion products is related to the accelerated kinetics of cathodic reactions, as already mentioned.

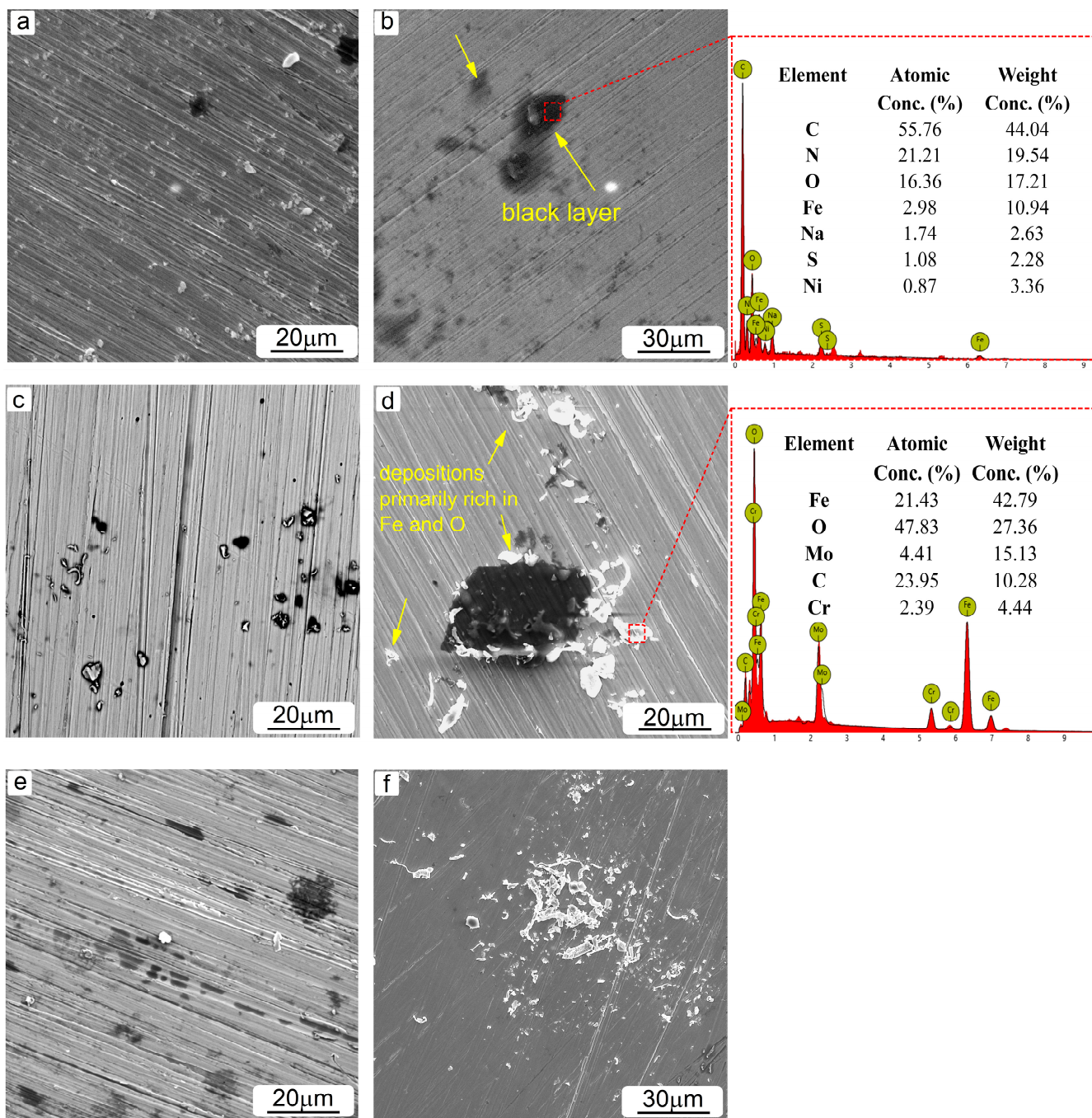
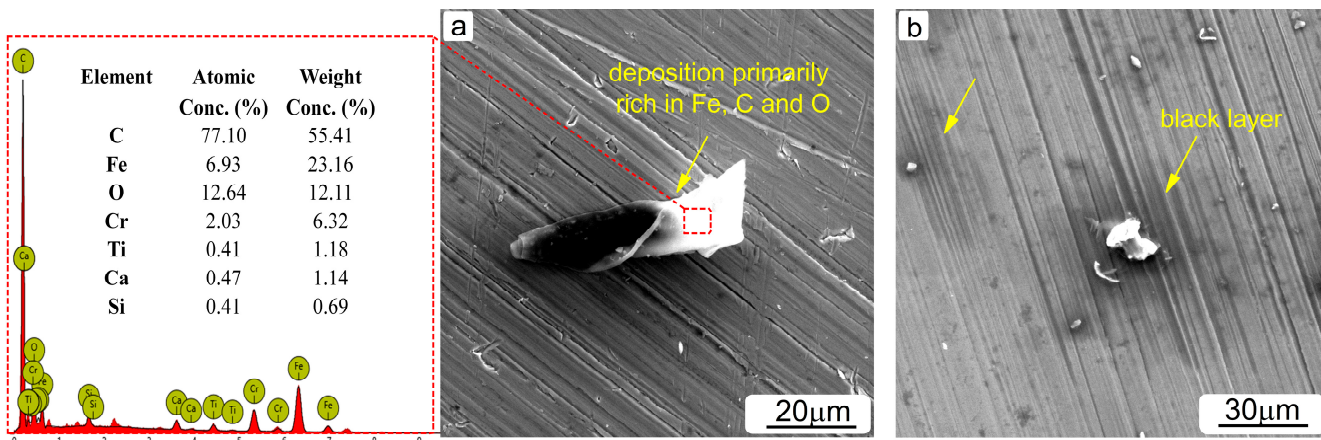


**Figure 6.** SEM images of SS 304L and SS 316L after potentiodynamic polarization tests in lean MEA-based solutions: (a,b) MEA at 25 °C and 40 °C, (c,d) MEA with SO<sub>X</sub> at 25 °C and 40 °C and (e,f) MEA with SO<sub>X</sub> and NO<sub>X</sub> at 25 °C and 40 °C.

### 3.4. Immersion Results

Potentiodynamic polarization experiments are of short duration, so the information they provide regarding both the development of a protective layer and the long-term corrosion behavior may not be representative of real conditions. For this reason, immersion experiments can offer a more comprehensive understanding of the behavior of the material when exposed to the corrosive medium for prolonged periods. Equation (15) was used as the basis for the technique to calculate the amount of weight loss:

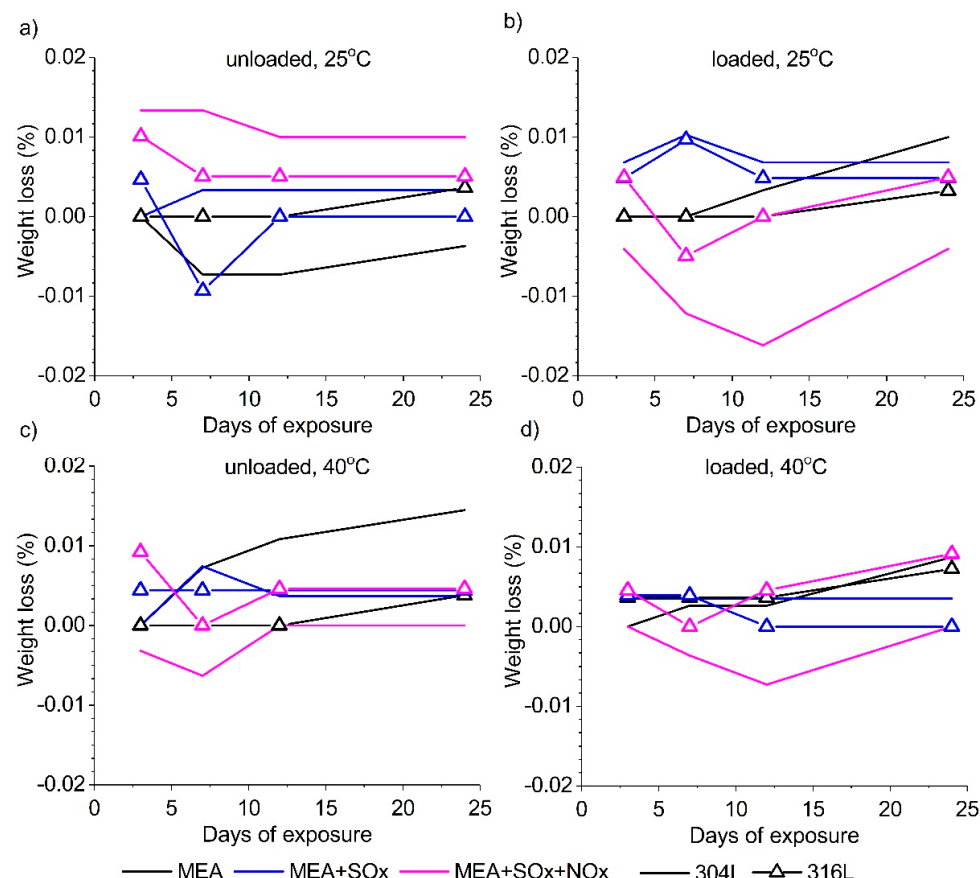
$$\text{weight loss} = (\text{initial weight} - \text{final weight})/\text{initial weight} \quad (15)$$



**Figure 7.** SEM images of specimens after potentiodynamic polarization tests in loaded MEA-based solutions.

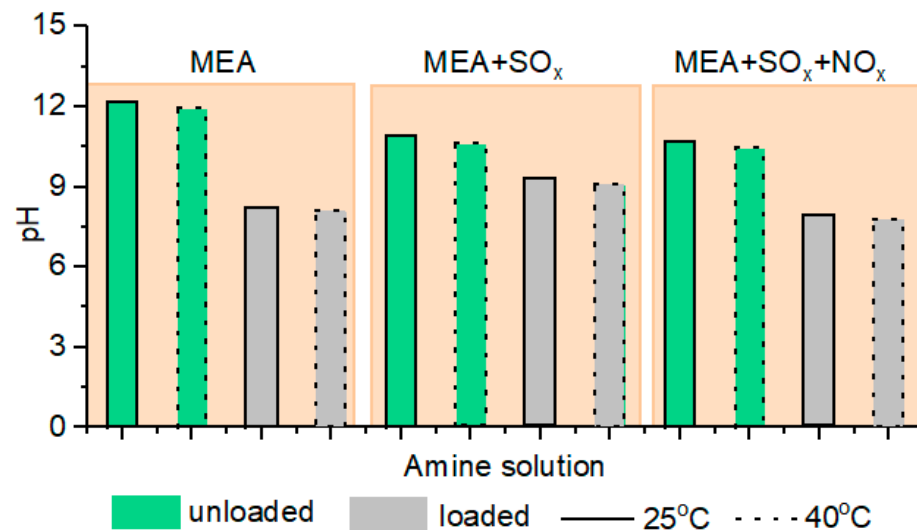
Generally, no significant weight change was observed across all specimens at any amine solution or temperature examined. Even after 24 days of exposure, any detected alteration was minimal, typically occurring at the third decimal point. While this limits the ability to draw significant conclusions from this method, it underscores the superior corrosion resistance exhibited by stainless steels when exposed to amine solvents.

Figure 8 presents the weight loss measurements of the SS 304L and SS 316L samples immersed in MEA-based solutions and evaluated at temperatures of 25 °C and 40 °C.



**Figure 8.** Weight loss measurements of SS 304L and SS 316L immersed in (a,b) unloaded and loaded MEA solutions at 25 °C and (c,d) unloaded and loaded MEA solutions at 40 °C.

The observations from immersion tests depicted in Figure 8 reveal that amine solutions containing either  $\text{SO}_x$  or a combination of  $\text{SO}_x$  and  $\text{NO}_x$  pollutants exhibit the capability to reduce the corrosion rate possibly by developing a passivation film on the metal surface, irrespective of the temperature and  $\text{CO}_2$  loading, for both SSs 304L and 316L. This is evident from the negative weight loss, indicating a net increase in material weight, as calculated using equation 15, or from the diminishing percentage of weight loss as the immersion duration extends. Previous studies on various steels have revealed that the presence of  $\text{SO}_4^{2-}$  contaminants leads to the formation of  $\text{FeSO}_4$ , which is further oxidized to  $\text{FeOOH}$  [37–40]. Another study showed that the presence of  $\text{NO}_3^-$  accelerates the corrosion rate at the initial stage, but then the rate reduces, probably due to the adsorption of degradation products that may have a synergistic effect with MEA. After several days of exposure, the film formed on the surface was composed of  $\alpha\text{-FeOOH}$  and an adsorption film from MEA degradation products [30]. The measurements of the solution's pH, shown in Figure 9, reveal that the introduction of  $\text{SO}_x$  and  $\text{NO}_x$  impurities, particularly  $\text{CO}_2$  loading, significantly increases the solution's acidity (i.e., the pH decreases). In contrast, a rise in temperature does not have a notable effect on the solution's acidity. Although low pH values initially increase the corrosion rate, the formation of a protective film is more likely to occur in solutions with a decreased pH [4]; thus, a solution's acidity plays a crucial role in metal protection. These results are consistent with the calculated corrosion rates and the findings from immersion tests in this research. Also, at both 25 °C and 40 °C, under lean and loaded MEA solution conditions, the two steel alloys demonstrated minimal corrosion rates during the initial days of immersion compared to the polluted MEA solutions, as evidenced by a nearly negligible weight loss. Conversely, the solutions contaminated with pollutants presented elevated corrosion rates, which is obvious from the significant weight reduction observed across almost all cases.



**Figure 9.** The pH measurements of the MEA-based solutions at 25 °C and 40 °C.

To verify the findings obtained from the immersion experiments, the surface morphology of certain corroded specimens underwent an examination using confocal microscopy, as presented in Figure 10. For comparison purposes, the morphology of an initial non-corroded specimen is also illustrated in Figure 10a. On the surface of the initial specimen, lines were present and were attributed to the grinding process, giving an  $R_z$  roughness value at 0.4  $\mu\text{m}$ . When immersed in lean or loaded MEA solutions, the specimen displayed minimal corrosion, and this was evident by the fact that its surface morphology hardly changed at all, closely resembling that of the specimen that did not undergo corrosion. Nevertheless, certain regions of the specimen, such as the one depicted in Figure 10b, exhibited discernible signs resembling small or bigger valleys, suggesting a localized form

of corrosion, which is likely attributed to the material's microstructural characteristics. When it comes to the lean and loaded MEA solutions contaminated with  $\text{SO}_X$  and  $\text{NO}_X$  pollutants, the surface analysis revealed multiple corrosion products differing in shape and size. Notably, in the illustration presented in Figure 10c, the maximum height of such corrosion products was determined to be  $h = 2.45 \mu\text{m}$ . The accumulation of these corrosion depositions can justify the tendency for stainless steel to increase its mass over time, as revealed by the immersion tests, in the amine solvent with pollutants.

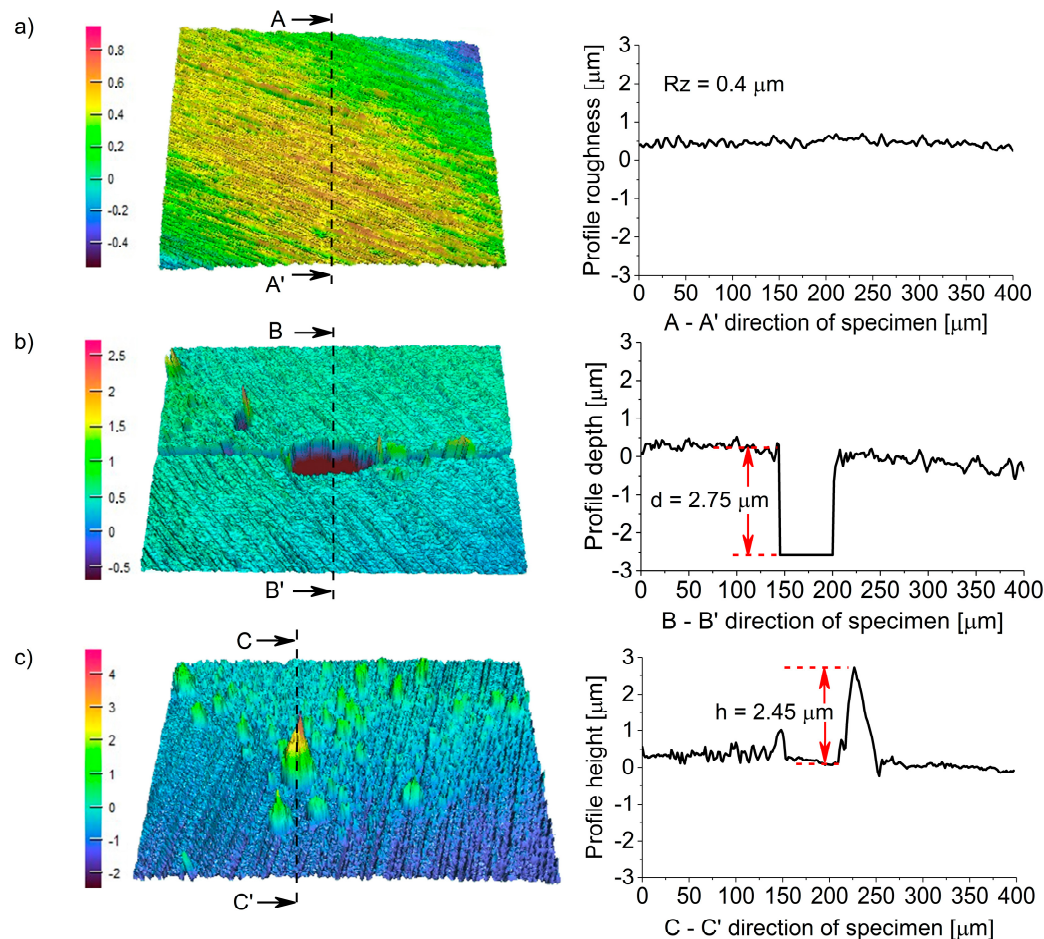


**Figure 10.** Optical profilometry images showing the surface topography of (a) a non-corroded specimen, (b) a corroded specimen in an MEA solution without pollutants and (c) in an MEA solution with pollutants.

#### 4. Conclusions

This study investigates the corrosion performance of SS 304L in a variety of pure or  $\text{SO}_X$ - and  $\text{NO}_X$ -contaminated MEA solutions, either lean or  $\text{CO}_2$ -loaded, at temperatures of 25 °C and 40 °C. An assessment of the experimental results revealed the following:

1. The  $\text{SO}_X$  and  $\text{NO}_X$  impurities had the strongest impacts on the corrosion rate over temperature and  $\text{CO}_2$  loading.
2. No pitting corrosion of SS 304L or SS 316L was detected in any of the examined solutions.
3. The microstructural characterization revealed the presence of various corrosion precipitations depending on the type of amine solution used. In lean MEA-based solutions, corrosion products rich in Fe and O were primarily formed, while the addition of  $\text{CO}_2$  further caused the formation of products containing Fe, O and C. Black layers likely composed of amine degradation products were identified in all solutions tested.

4. The weight loss measurements showed a very low corrosion rate in all solutions at both temperatures. Also, the results reveal that maybe SO<sub>X</sub> and NO<sub>X</sub> impurities are responsible for the formation of a protective layer.

**Author Contributions:** Conceptualization, F.S. and N.M.; methodology, F.S. and E.N.; software, E.L.; validation, E.L. and F.S.; formal analysis, E.L.; investigation, G.S. and E.L.; resources, N.M.; data curation, G.S. and E.L.; writing—original draft preparation, E.L. and F.S.; writing—review and editing, F.S.; visualization, E.L.; supervision, N.M.; project administration, A.I.P.; funding acquisition, P.S. All authors have read and agreed to the published version of the manuscript.

**Funding:** This research was financed by the European Union and Greek National Funds through the Operational Program Competitiveness, Entrepreneurship and Innovation under Research-CREATE-Innovate, Project T2EΔK-01911.

**Institutional Review Board Statement:** Not applicable.

**Informed Consent Statement:** Not applicable.

**Data Availability Statement:** Data are contained within the article.

**Conflicts of Interest:** The authors declare no conflicts of interest.

## References

1. Santos, S.P.D. *Comparative Study of Amine Solutions Used in Absorption/Desorption Cycles of CO<sub>2</sub>*; LAP Lambert Academic Publishing: Saarbrücken, Germany, 2014.
2. Madejski, P.; Chmiel, K.; Subramanian, N.; Kuś, T. Methods and Techniques for CO<sub>2</sub> Capture: Review of Potential Solutions and Applications in Modern Energy Technologies. *Energies* **2022**, *15*, 887. [[CrossRef](#)]
3. Aghel, B.; Janati, S.; Wongwises, S.; Shadloo, M.S. Review on CO<sub>2</sub> capture by blended amine solutions. *Int. J. Greenh. Gas Control* **2022**, *119*, 103715. [[CrossRef](#)]
4. Zheng, L.; Matin, N.S.; Landon, J.; Thomas, G.A.; Liu, K. CO<sub>2</sub> loading-dependent corrosion of carbon steel and formation of corrosion products in anoxic 30wt.% monoethanolamine-based solutions. *Corros. Sci.* **2016**, *102*, 44–54. [[CrossRef](#)]
5. Meng, F.; Meng, Y.; Ju, T.; Han, S.; Lin, L.; Jiang, J. Research progress of aqueous amine solution for CO<sub>2</sub> capture: A review. *Renew. Sustain. Energy Rev.* **2022**, *168*, 112902. [[CrossRef](#)]
6. Zhao, F.; Cui, C.; Dong, S.; Xu, X.; Liu, H. An overview on the corrosion mechanisms and inhibition techniques for amine-based post-combustion carbon capture process. *Sep. Purif. Technol.* **2023**, *304*, 122091. [[CrossRef](#)]
7. Saeed, I.M.; Alaba, P.; Mazari, S.A.; Basirun, W.J.; Lee, V.S.; Sabzoi, N. Opportunities and challenges in the development of monoethanolamine and its blends for post-combustion CO<sub>2</sub> capture. *Int. J. Greenh. Gas Control* **2018**, *79*, 212–233. [[CrossRef](#)]
8. Nwaoha, C.; Supap, T.; Idem, R.; Saiwan, C.; Tontiwachwuthikul, P.; AL-Marri, M.J.; Benamor, A. Advancement and new perspectives of using formulated reactive amine blends for post-combustion carbon dioxide (CO<sub>2</sub>) capture technologies. *Petroleum* **2017**, *3*, 10–36. [[CrossRef](#)]
9. Veawab, A.; Tontiwachwuthikul, P.; Chakma, A. Corrosion Behavior of Carbon Steel in the CO<sub>2</sub> Absorption Process Using Aqueous Amine Solutions. *Ind. Eng. Chem. Res.* **1999**, *38*, 3917–3924. [[CrossRef](#)]
10. Emori, W.; Jiang, S.L.; Duan, D.L.; Ekerenam, O.O.; Zheng, Y.G.; Okafor, P.C.; Qiao, Y.X. Corrosion behavior of carbon steel in amine-based CO<sub>2</sub> capture system: Effect of sodium sulfate and sodium sulfite contaminants. *Mater. Corros.* **2016**, *68*, 674–682. [[CrossRef](#)]
11. Kittel, J.; Gonzalez, S. Corrosion in CO<sub>2</sub> Post-Combustion Capture with Alkanolamines—A Review. *Oil Gas Sci. Technol.-Rev. D'ifp Energ. Nouv.* **2014**, *69*, 915–929. [[CrossRef](#)]
12. Fang, Z.; Roy, K.; Padiyara, S.; Chen, B.; Raftery, G.M.; Lim, J.B.P. Web crippling design of cold-formed stainless steel channels under interior-two-flange loading condition using deep belief network. *Structures* **2023**, *47*, 1967–1990. [[CrossRef](#)]
13. Feng, R.; Pan, J.; Zhang, J.; Shao, Y.; Chen, B.; Fang, Z.; Roy, K.; Lim, J.B.P. Effects of corrosion morphology on the fatigue life of corroded Q235B and 42CrMo steels: Numerical modelling and proposed design rules. *Structures* **2023**, *57*, 105136. [[CrossRef](#)]
14. Rafat, A.; Atilhan, M.; Kahraman, R. Corrosion Behavior of Carbon Steel in CO<sub>2</sub> Saturated Amine and Imidazolium-, Ammonium-, and Phosphonium-Based Ionic Liquid Solutions. *Ind. Eng. Chem. Res.* **2016**, *55*, 446–454. [[CrossRef](#)]
15. Veawab, A.; Aroonwilas, A. Identification of oxidizing agents in aqueous amine–CO<sub>2</sub> systems using a mechanistic corrosion model. *Corros. Sci.* **2002**, *44*, 967–987. [[CrossRef](#)]
16. Xiang, Y. Corrosion issues of carbon capture, utilization, and storage. *Mater. Perform.* **2018**, *57*, 32–35.
17. Xiang, Y.; Yan, M.; Choi, Y.-S.; Young, D.; Nesic, S. Time-dependent electrochemical behavior of carbon steel in MEA-based CO<sub>2</sub> capture process. *Int. J. Greenh. Gas Control* **2014**, *30*, 125–132. [[CrossRef](#)]
18. Ooi, Z.L.; Tan, P.Y.; Tan, L.S.; Yeap, S.P. Amine-based solvent for CO<sub>2</sub> absorption and its impact on carbon steel corrosion: A perspective review. *Chin. J. Chem. Eng.* **2020**, *28*, 1357–1367. [[CrossRef](#)]

19. Wang, Y.; Fang, M.; Wang, T.; Gao, J.; Huang, Y.; Li, S.; Lu, X.; Sun, Y.; Zhang, F. Corrosion performance of carbon/stainless steel in amine-based solvents under different conditions for CO<sub>2</sub> chemical absorption process. *Greenh. Gases Sci. Technol.* **2023**, *14*, 26–41. [[CrossRef](#)]
20. Stergioudi, F.; Baxevani, A.; Florou, C.; Michailidis, N.; Nessi, E.; Papadopoulos, A.I.; Seferlis, P. Corrosion Behavior of Stainless Steels in CO<sub>2</sub> Absorption Process Using Aqueous Solution of Monoethanolamine (MEA). *Corros. Mater. Degrad.* **2022**, *3*, 422–438. [[CrossRef](#)]
21. Sun, Y.; Remias, J.; Neathery, J.; Liu, K. Electrochemical study of corrosion behaviour of carbon steel A106 and stainless steel 304 in aqueous monoethanolamine. *Corros. Eng. Sci. Technol.* **2011**, *46*, 724–731. [[CrossRef](#)]
22. ASTM G38-01; Standard practice for Preparing, Cleaning, and Evaluating Corrosion Test Specimens. ASTM International: West Conshohocken, PA, USA, 2003.
23. Tzirakis, F.; Tsivintzelis, I.; Papadopoulos, A.I.; Seferlis, P. Experimental measurement and assessment of equilibrium behaviour for phase change solvents used in CO<sub>2</sub> capture. *Chem. Eng. Sci.* **2019**, *199*, 20–27. [[CrossRef](#)]
24. Sim, S.; Corrigan, P.; Cole, I.S.; Birbilis, N. Use of Aqueous Solutions to Simulate Supercritical CO<sub>2</sub> Corrosion. *Corrosion* **2012**, *68*, 045004-1–045004-11. [[CrossRef](#)]
25. Ghalib, L.; Ali, B.S.; Mazari, S.; Saeed, I.M. Modeling the Effect of Piperazine on Carbon Steel Corrosion Rate in Carbonated Activated MDEA Solutions. *Int. J. Electrochem. Sci.* **2016**, *11*, 4560–4585. [[CrossRef](#)]
26. Wattanaphan, P. *Studies and Prevention of Carbon Steel Corrosion and Solvent Degradation During Amine-Based CO<sub>2</sub> Capture from Industrial Gas Streams*; The University of Regina: Regina, SK, Canada, 2012.
27. Pierre, R.R. *Handbook of Corrosion Engineering*; McGraw Hill Professional: New York, NY, USA, 1999; Chapter 2; p. 67.
28. Widjanto, B.; Putri, S. Corrosion Behavior of ASTM A1008 Carbon Steel in Mixtures of HNO<sub>3</sub>, H<sub>2</sub>SO<sub>4</sub>, and HCl Using Immersion and Polarization Methods. *Mater. Trans.* **2019**, *60*, 732–736. [[CrossRef](#)]
29. Mohammed, H.K.; Jafar, S.A.; Humadi, J.I.; Sehgal, S.; Saxena, K.K.; Abdullah, G.H.; Saeed, L.I.; Salman, M.S.; Abdullah, W.S. Investigation of carbon steel corrosion rate in different acidic environments. *Mater. Today Proc.* **2023**. [[CrossRef](#)]
30. Xiang, Y.; Xie, W.; Ni, S.; He, X. Comparative study of A106 steel corrosion in fresh and dirty MEA solutions during the CO<sub>2</sub> capture process: Effect of NO<sup>3-</sup>. *Corros. Sci.* **2020**, *167*, 108521. [[CrossRef](#)]
31. Lekatou, A.; Sioulas, D.; Karantzalis, A.E.; Grimanelis, D. A comparative study on the microstructure and surface property evaluation of coatings produced from nanostructured and conventional WC-Co powders HVOF-sprayed on Al7075. *Surface Coat. Technol.* **2015**, *276*, 539–556. [[CrossRef](#)]
32. Esmailzadeh, S.; Aliofkhazraei, M.; Sarlak, H. Interpretation of Cyclic Potentiodynamic Polarization Test Results for Study of Corrosion Behavior of Metals: A Review. *Prot. Met. Phys. Chem. Surf.* **2018**, *54*, 976–989. [[CrossRef](#)]
33. Scheiman, M.A. *A Review of Monoethanolamine Chemistry*; U.S. Naval Research Laboratory: Washington DC, USA, 1962; Available online: <https://apps.dtic.mil/sti/tr/pdf/AD0277031.pdf> (accessed on 15 January 2024).
34. Dixon, B.E.; Williams, R.A. Reaction of iron with monoethanolamine. *J. Chem. Technol. Biotechnol.* **1950**, *69*, 69–71. [[CrossRef](#)]
35. Fostås, B.; Gangstad, A.; Nenseter, B.; Pedersen, S.; Sjøvoll, M.; Sørensen, A.L. Effects of NOx in the flue gas degradation of MEA. *Energy Procedia* **2011**, *4*, 1566–1573. [[CrossRef](#)]
36. Li, X.; Pearson, P.; Yang, Q.; Puxty, G.; Feron, P.; Xiao, D. A study of designer amine 4-amino-1-propyl-piperidine against the corrosion of carbon steel for application in CO<sub>2</sub> capture. *Int. J. Greenh. Gas Control* **2020**, *94*, 102929. [[CrossRef](#)]
37. Sun, C.; Sun, J.; Wang, Y.; Lin, X.; Li, X.; Cheng, X.; Liu, H. Synergistic effect of O<sub>2</sub>, H<sub>2</sub>S and SO<sub>2</sub> impurities on the corrosion behavior of X65 steel in water-saturated supercritical CO<sub>2</sub> system. *Corros. Sci.* **2016**, *107*, 193–203. [[CrossRef](#)]
38. Dugstad, A.; Halseid, M.; Morland, B. Effect of SO<sub>2</sub> and NO<sub>2</sub> on Corrosion and Solid Formation in Dense Phase CO<sub>2</sub> Pipelines. *Energy Procedia* **2013**, *37*, 2877–2887. [[CrossRef](#)]
39. Xiang, Y.; Wang, Z.; Xu, C.; Zhou, C.; Li, Z.; Ni, W. Impact of SO<sub>2</sub> concentration on the corrosion rate of X70 steel and iron in water-saturated supercritical CO<sub>2</sub> mixed with SO<sub>2</sub>. *J. Supercrit. Fluids* **2011**, *58*, 286–294. [[CrossRef](#)]
40. Xu, M.; Zhang, Q.; Wang, Z.; Liu, J.; Li, Z. Effect of High-Concentration O<sub>2</sub> on Corrosion Behavior of X70 Steel in Water-Containing Supercritical CO<sub>2</sub> with SO<sub>2</sub>. *Corrosion* **2016**, *73*, 290–302. [[CrossRef](#)]

**Disclaimer/Publisher's Note:** The statements, opinions and data contained in all publications are solely those of the individual author(s) and contributor(s) and not of MDPI and/or the editor(s). MDPI and/or the editor(s) disclaim responsibility for any injury to people or property resulting from any ideas, methods, instructions or products referred to in the content.